ECS Transactions, 78 (1) 3349-3363 (2017)
10.1149/07801.3349ecst ©The Electrochemical Society

Advanced Proton Conducting Ceramic Cell as Energy Storage Device

M. Marrony and J. Dailly

[a] European Institute for Energy Research
Emmy-Noether Strasse 11, Karlsruhe, 76131, Germany

Ba-based protonic ceramic cell (PCC) was investigated under galvanostatic electrolysis and reversible fuel cell / electrolysis cycles modes. Such PCC has been made by industrial wet chemical routes (tape casting and screen-printing methods) and by using NiO-$BaCe_{0.8}Zr_{0.1}Y_{0.1}O_{3-\delta}$ (BCZY81) as anode material layer / BCZY81–ZnO (5 mol%) as electrolyte, $Ba_{0.5}Sr_{0.5}Co_{0.8}Fe_{0.2}O_{3-\delta}$ (BSCF) – BCZY81) as air electrode and BSCF as current collector. The optimization of key parameters of both fuel cell and electrolysis operating conditions such as water feed content, fuel utilization, temperature operation allow to validating promising electrical cell performances (>0.25 W/cm², 0.7V under fuel cell mode; 0.5A/cm², 1.3V under electrolysis mode) and reliability during more than 3500 h with limited electrical degradation (<2%/kh) at 700°C. The evolution of on line Electrochemical Impedance Spectroscopy measurements reveals that the total electrical resistances of PCC are lower under electrolysis mode than under fuel cell mode, in particular the ohmic resistance (electrolyte). But in the same time, the polarization resistance of the cell (air electrode interface) is higher under electrolysis mode. With time, the combination of high temperature and water vapor pressure can induce negative reaction able to accelerate the Ba-based materials aging. In any case, such highlights pave the way to the use of PCC technology as high efficient energy storage candidate.

Introduction

The last decade reveals the high potential of Solid oxide cells (SOC) as hydrogen battery storage operating to the demand either under fuel cell (concept gas-to-power) or electrolysis (concept power-to-gas) profiles. Such types of ceramic-based cells usually operate beyond 750°C in order to keep reasonable electrical performances and reliability of the whole electrochemical device. Now, one of the main challenges is to reduce the operating temperature in order to limit ageing parameters (Cr contamination, metal corrosion…) and improve energy efficiency while promoting cheaper materials and system processing. Actually, O^{2-}-conducting SOC suffers to an insufficient activity of the oxygen electrode and electrical performances at lower operation temperature.

In such aspect, Protonic Ceramic Cell (PCC) technology can overcome main technical hurdles while operating below 700°C, in particular by reducing critical ageing and chemical reactivity of materials used as cell and stack components. In addition,

proton conducting ceramic-based cells benefit from the presence of the water produced/consumed at the air electrode side, avoiding the dilution of the fuel and by this way optimizing the electric efficiency of the system. Thus, PCC is now widely investigated for a variety of applications, in particular fuel cell (1-4), steam electrolysis (5-7) and hydrogen separation (8-10) but such technology has to face to the lack of Technology Readiness Level (non-well defined operating parameters conditions, poor return of experiments for durability, poor stack cell dimensioning research…) for a viable way of market. Among all ceramic materials studied, perovskite Ba-based oxides keep the leadership as electrolyte or electrodes into optimized lab-scaled cell fabrication processes (11-12). In particular, our group validated recent promising electrical performances beyond 400 mW/cm² at 600-700°C and reliability of few hundred hours under dynamic fuel cell power demand profile (13-15). In such context, here is discussed the evaluation of advanced Ba-based PCC materials and manufacturing processes under electrolysis and flexible reversible Fuel cell / electrolysis cycles modes.

Experimental

Anode slurry was prepared by mixing powders ($BaCe_{0.8}Zr_{0.1}Y_{0.1}O_{3-\delta}$ (BCZY81) (Cerpotech A.S.) / NiO (J.T. Baker ®) 40:60 wt %), solvents (Ethanol/MEK) and a dispersing agent in a Turbula® type T2F (WAB). After 24 hours of mixing, polyvinyl butyral binder and two plasticizers were added, then the solution was mixed for 3 hours. After one day standing period, air was removed from the slurry using a vacuum process. The slurry was then casted on a silicon coated PET film using a ZAA 2300 automatic film applicator coater (Zehntner GmbH, Switzerland), and then dried for 12 hours at room temperature, in a confined box under ventilation to help removing solvent vapors.

Electrolyte ink was composed of ceramic BCZY81 powder (Cerpotech A.S.) mixed with 5mol% of ZnO (Sigma-Aldrich)) in a mixture composed of 6wt% of ethylcellulose (Sigma Aldrich) in terpineol (Alfa Aesar). Two BCZY81-ZnO layers were coated by screen-printing onto the top of the anode substrate followed by a drying step at 60°C before a sintering step at 1400°C/9h. An ironing step at 1350°C was necessary to improve the flatness of the half-cell. Air electrode was also coated by screen-printing. The two layers' electrode was composed of a first composite layer of BSCF (Marion Technologies)/BCZY81 (80:20 wt. %) powders. The current collector upper layer was composed of pure BSCF, which electronic conductivity is sufficient and chemically stable and compatible with the composite layer. Both inks were prepared as the electrolyte ink (mixture of ceramic powders with a vehicle composed of 6wt.% ethylcellulose into terpineol). After a drying step at 60°C, the cathode was sintered at 1100°C for one hour.

Single cells were tested in a Fiaxell® Open Flange test bench at 700°C. During both fuel cell and electrolysis steps, purified water was added on the air side using a Neolab® mini-pump while hydrogen gas is introduced on the anode side. The current collection was performed using gold wires connected to a gold mesh at the air side and nickel wires connected to a nickel mesh at the fuel side.

Electrochemical measurements (IV and IP curves) were carried out with the software CorrWare®. Electrochemical Impedance Spectroscopy measurements were obtained over the frequency range from 0.31 to 103 Hz using a Solartron FRA 1255 and the software

ZPlot®. External morphologies of the cell were studied by electron microscopy in a field-emission scanning secondary electron microscope.

The activation step corresponds to the initial heating ramp to 700°C (under nitrogen and air at the fuel and air electrode, respectively), to the reduction of the nickel oxide while introducing hydrogen at the fuel electrode and to a galvanostatic period under fuel cell condition to stabilize the potential of the cell at 0.7V. Then, an endurance test is made with such PCC by including four dynamic types of operation profile: two ones related to steam water electrolysis and done under galvanostatic mode and two other ones related to reversible dynamic operation. More specifically, steam water electrolysis operations were carried out at E=1.2V with a steam water conversion calculated to 84% (air: 18.7 l/h + H_20: 7 vol%; H_2: 3 l/h). The fuel cell mode was operated under dry gases with a fuel efficiency calculated to 30% (air: 18.7 l/h; H_2: 4.4 l/h). The two reversibility profiles consist in successive cycles between fuel cell (E=0.80V) and electrolysis (E=1.20V) operating conditions, e.g. electricity and hydrogen production. The differences between the two profiles are related to the frequency of cycle steps (see Figure 1).

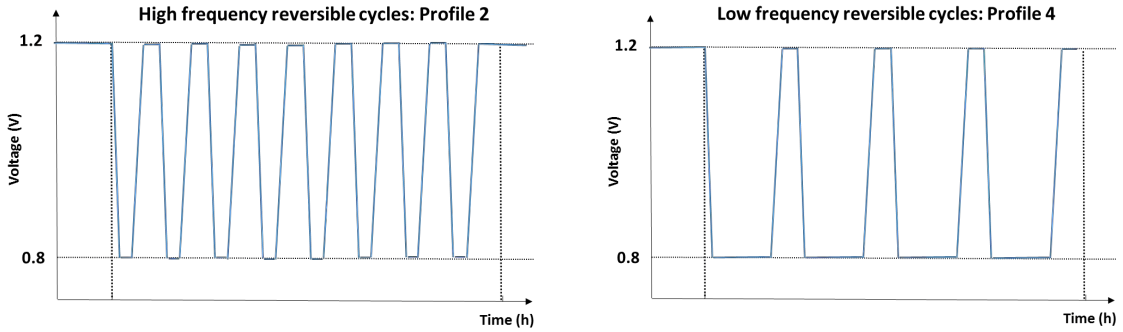

Figure 1. Evolution of the potential and description of the reversible fuel cell/electrolysis cycles profiles.

Here are summarized the successive profiles studied:

- Profile 1: the cell is operating under galvanostatic electrolysis mode at -0.3A/cm²
- Profile 2: the PCC is operating under high frequency reversible fuel cell/electrolysis power cycles with 100 h of stabilization at each sequence of cycle,
- Profile 3: the cell is operating under galvanostatic electrolysis mode at -0.3 A/cm²,
- Profile 4: low frequency reversible cycles were performed with larger endurance sequences (>100 h) under fuel cell mode.

IV-curves and impedance spectra measured under fuel cell operation at 0.3 A/cm² have been performed at each beginning of the test profile (BoT) and at each end of the test profile (EoT) in order to estimate the impact of such operating conditions on the electrical performance of the cell, i.e. to calculate the degradation of the potential with time.

Electrical resistance values of the cell were deduced from typical Nyquist plots of the impedance. The high-frequency intercept corresponds to the Ohmic resistance (ASR_Ω), whereas the low-frequency intercept is the total resistance of the cell (ASR_{tot}). Thus the

polarisation resistance (ASR_{pol}) of the electrodes is deduced from the two previously defined resistances by following the equation:

$$ASR_{tot} = ASR_{\Omega} + ASR_{pol} \quad [1]$$

In parallel, ASR_{tot} has been also deduced from the slope of the IV-curve. All the values measured under various profile are reported in the Table I (open circuit voltage OCV, power density and Area Specific Resistance ASR).

Results and Discussion

A 4.5x4.5 (20.25) cm^2 cell was prepared with a current collector active area of 10.75 cm^2 (Figure 2).

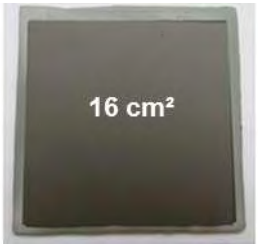

Figure 2. Picture of the BCZY81/BSCF-based 20 cm² sized cell with a 4x4 cm² air electrode

Figure 3 shows the evolution of the voltage and current during the whole endurance test. A full test of about 3500 hours has been performed at 700°C under specified operation conditions.

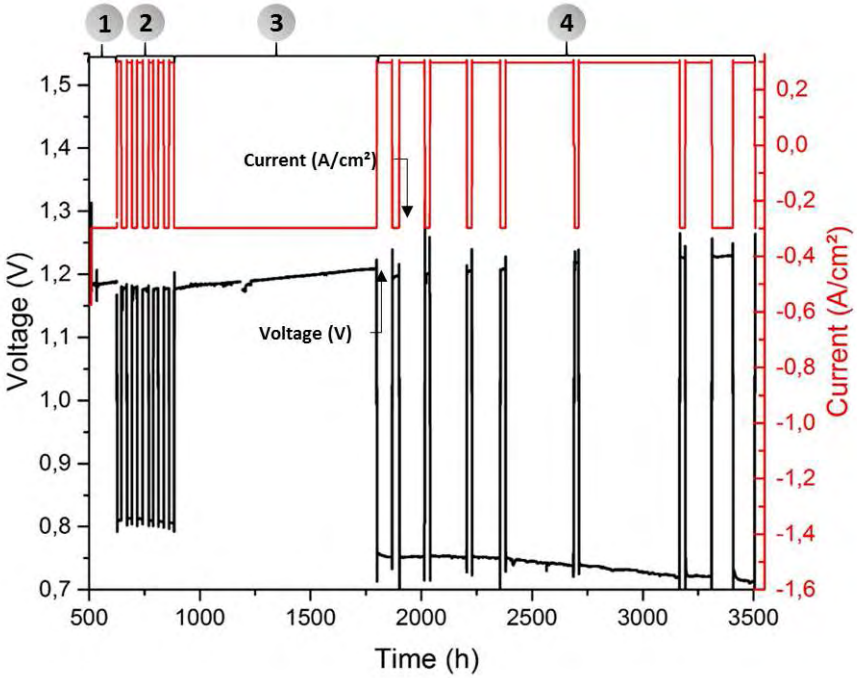

Figure 3. Evolution of the potential and description of the different profiles.

Initial Electrochemical Characterizations

An initial electrochemical characterization of both fuel cell and electrolysis profiles (IV and IP curves) is performed after the activation phase in order to estimate the electrical performance and the physic-chemical strength of the cell at the beginning of the test. The figure 4a describes a high open circuit voltage (OCV) measured beyond 1V at 700°C under fuel cell profile. Close to the standard potential value to form water from the electrochemical H_2/O_2 reaction (i.e. 1.23V), such experimental value reveals no real gas-tight phenomena for the cell, and in particular a well-densified BCZY81 electrolyte layer.

a)

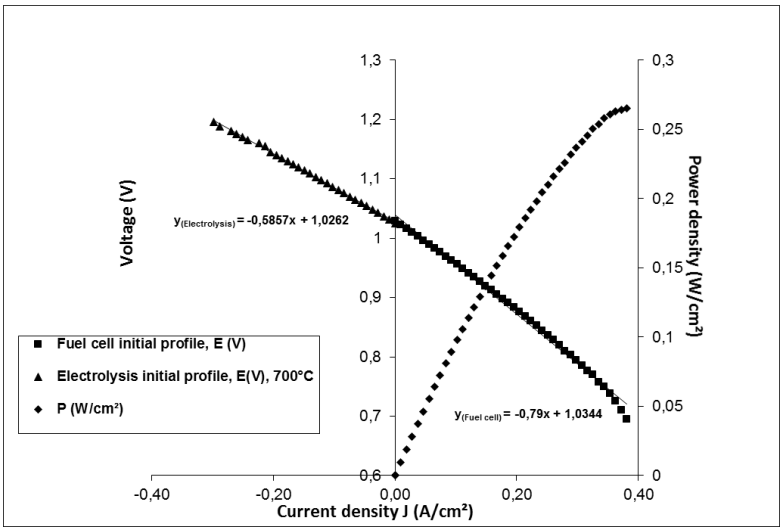

b)

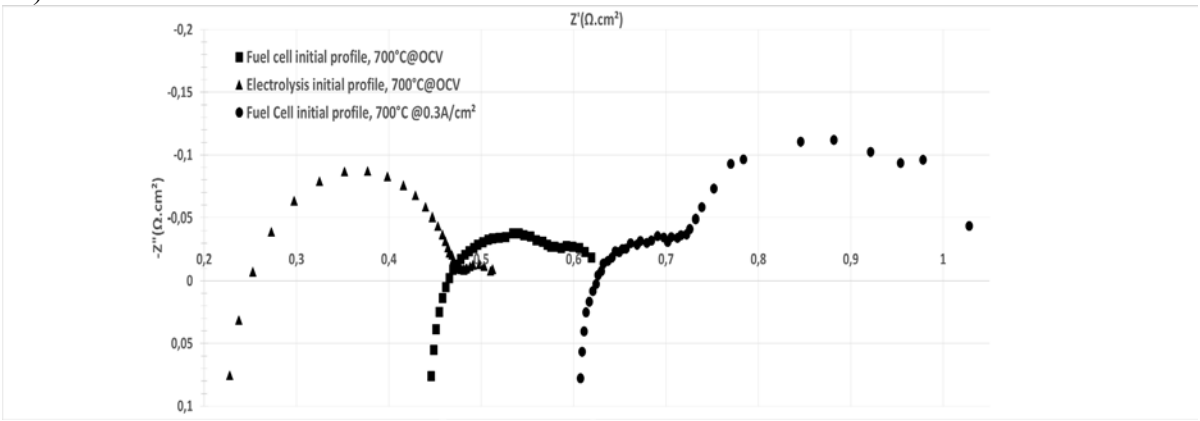

Figure 4. Polarization curve of a 16cm² NiO-BCZY81/BCZY81-ZnO/BSCF-BCZY81/BSCF cell during the initial fuel cell operation.

A power density of 0.27 $W.cm^{-2}$ is measured at E=0.7V. The conductivity of the electrolyte has been deduced from the area specific resistance value of the impedance spectra measured under current (figure 4b). It is estimated to $\sigma=2.10^{-4}$ $S.cm^{-1}$, which is significantly below than the value found in the literature (10^{-3} $S.cm^{-1}$) (16). Such gap can be partially explained by the difference between the operation conditions, in particular the humidification of hydrogen atmosphere on the intrinsic proton conduction properties of the electrolyte layer and between the electrolyte material characteristics (lower doping value of yttrium in our case, measurement under powder pellet versus a complete cell in our case). In addition, a rapid comparison of impedance spectra of the cell operating

under fuel cell profile and measured at OCV and under current (0.3 A/cm²) reveals an increase of total resistance from 0.63 to 1.04 Ω.cm², mainly caused by the increase of the polarization resistance of electrodes and interfaces during the oxygen reduction reaction (ORR) for water formation (figure 1b). Under electrolysis mode, a voltage value of 1.18V is reached at -0.3 A/cm² (figures 1a). The total resistance of the cell calculated by the slope of the IV curve is lower when the cell is running under electrolysis mode than under fuel cell mode ($ASR_{tot,\ Electrolysis}$=0.59 Ω.cm² and $ASR_{tot,\ Fuel\ Cell}$=0.79 Ω.cm², respectively). More specifically, the analysis of impedance spectra (figure 1b) reveals the ohmic resistance value mainly brought by the electrolyte layer significantly lower when the cell is running under electrolysis operation versus the fuel cell mode. Relative high water content exposure (electrolysis profile) could be a benefit for better proton diffusion/concentration through dense electrolyte layer and reduce the ohmic resistance of the cell. Even more, from the shape of the impedance spectra in the medium frequency, it can be deduced that the polarization resistance value related to the contribution of the electrode interfaces is higher under electrolysis than fuel cell modes. The variation of operating parameter keys of the test, in particular the fuel utilization and steam water content, could induce variations in the electrical resistance responses related to ORR mechanism of the PCC air electrode interface. Thus, in our case, PCC air electrode layer would suffer lower in a role of water production at moderate voltage (0.5-1 V) (fuel cell profile) than of water splitting at higher voltage (>1V) (electrolysis profile).

TABLE I. OCV and ASRs 700°C vs. test operating conditions measured at OCV

Operation conditions	OCV (V)	IV-Curve	Electrochemical Impedance spectroscopy measurement @OCV		
		ASR_{tot} (Ω.cm²)	ASR_{Ω} (Ω.cm²)	ASR_{pol} (Ω.cm²)	ASR_{tot} (Ω.cm²)
Initial (fuel cell)	1.03	0.79	0.47	0.16	0.63
Initial (electrolysis)	1.01	0.56	0.25	0.26	0.51

The cell electrical performances are described and analysed in the following sections under the four dynamic profiles selected:

Profile 1 Electrochemical Characterizations

The profile 1 investigated the impact of steam water electrolysis conditions on the electrical performances and reliability of Ba-based proton conducting ceramic cell. Indeed, it is well admitted the relative reactivity of Ba elements under hydrophilic atmosphere with a high substitution level of the Zr-site to form barium hydroxide. But such study was only made on powder pellets shape and under harsh condition and has to be confirmed under real cell operation (17). In a classical steam water electrolysis operation of high temperature solid oxide cell, three types of operation modes can be distinguished: thermoneutral, endothermal, and exothermal. When the cell operates at thermal equilibrium (~1.28 V at 700 °C), the electrical energy input equals the total energy demand and the electrical-to-hydrogen conversion efficiency is 100 %. Moreover, the heat demand Q = TΔS (with T: temperature of operation and ΔS the enthalpy of reaction) necessary for the water splitting equals the heat released by the joule heating (ohmic losses) within the cell. Under the exothermal mode, the electric energy input exceeds the enthalpy of reaction, corresponding to an electrical efficiency below 100 %. In such mode, heat is generated from the cell and can be reused in the system to preheat the inlet gases. This mode has also the advantage to operate at higher current density

allowing potentially decreasing the size of the system. However, empirical results highlighted that such exothermal mode can induce a source of prematurely ageing of the cell components. Under the endothermal mode, the electric energy input stays below the enthalpy of reaction which means a cell voltage below the thermoneutral one. Therefore, heat must be supplied to the system to maintain the temperature. Such mode means theoretical electrical-to-hydrogen conversion efficiencies of the PCC above 100 %. This operation mode also allows minimal long-term degradation rates, since it is achieved at the lowest power densities. Thus, it has been chosen to do operate the cell under galvanostatic endothermal mode. For that, the current density was fixed at BoT profile at -0.3 A/cm² so that the potential of the cell can initially achieve 1.15 V, i.e. below the thermoneutral potential region of the cell. Steam water electrolysis profile is followed for about 200 hours. Figure 5 compares the evolution of the IV curves and the corresponding electrochemical impedance spectra of PCC measured at BoT and EoT during such operation.

a.

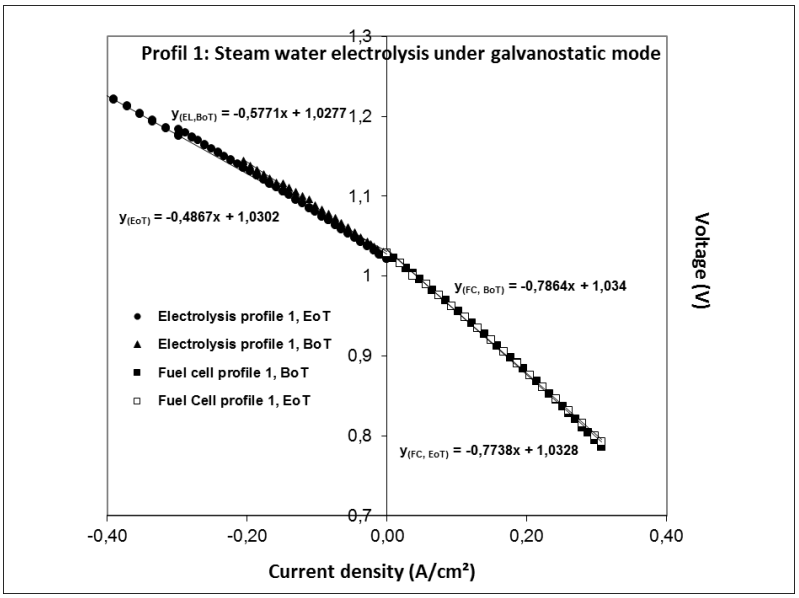

b.

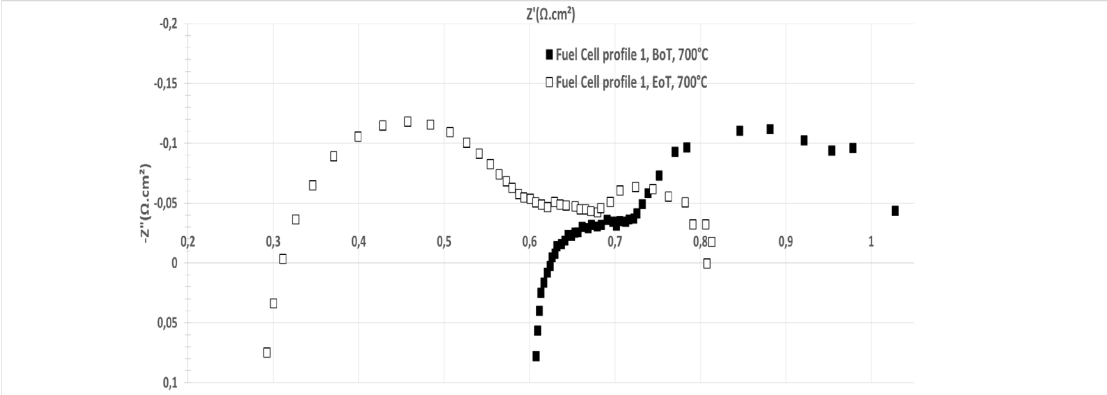

Figure 5. a) Polarization curve and b) Impedance spectra under polarization of a 16cm² sized NiO-BCZY81/BCZY81-ZnO/BSCF-BCZY81/BSCF cell during profile 1.

From the I-V curves of figure 5a, we can notice a high and constant open circuit voltage of the cell kept along the steam water electrolysis static profile duration. It indicates that the electrolyte is still well gas tight after the end of the profile without any

noticeable electrical degradation of the cell voltage measured at -0.3 A/cm². But more specifically, the analysis of impedance spectra measured before and after the test profile (figure 5b) reveals a significant decrease of ohmic resistance of the cell almost compensated by a small increase of the polarization resistance in parallel. The intrinsic electrical properties of the electrolyte layer would be improved while in the same time, the interface to the electrodes would suffer to such electrolysis operating condition. At such stage, we would admit that the galvanostatic electrolysis mode induces a negative impact on the composite air electrode interface layer polarization resistance related to the ORR water splitting mechanism. In the same time, a relative high steam water exposure could support higher activation of intrinsic proton diffusion / concentration properties of the electrolyte layer. Indeed, the water molecules, dissociated on the oxygen-deficient host perovskite structure should fill the oxygen vacancies and could be an added source of protons as described by Colomban et al (17). In any case, such observations confirm the postulate that the combination of high temperature and high water vapor pressure allows an increase in proton conductivity of BCZY81 material used in the electrolyte and in the composite layers, but can also promote the advancement of reaction with water, and hence induce material aging (18).

Profile 2 Electrochemical Characterizations:

The second operation profile allowed to validating six reversible fuel cell/electrolysis cycles in 300 hours of test (Figure 6a). During such period, the electrical degradation of the cell voltage was reaching -1.7%/kh.

The IV curves measured at BoT and EoT (see figure 6b) describes a contrast in the cell performance evolution with a smooth decrease noticed under fuel cell mode (after the cycle 1) and an increase (until an asymptotic profile from the cycle 3) under electrolysis mode. Such observation is nearly confirmed by the impedance spectra analysis of the cell measured under fuel cell profile before and after the test by a quite stable total resistance value (Figure 6c, Table II). However, the electrical resistances contribution is now changing with a significant increase of the ohmic resistance while the polarization resistance is slightly reduced. Under such dynamic voltage profile, the fuel cell mode made under dry inlet gases would allow to alleviating the negative impact of high water exposure of the electrolysis mode on the Ba-based perovskite electrolyte structure. In between, we confirm the observation that the air electrode interface still suffers higher under electrolysis mode (water splitting reaction) than under fuel cell mode (water production).

a.

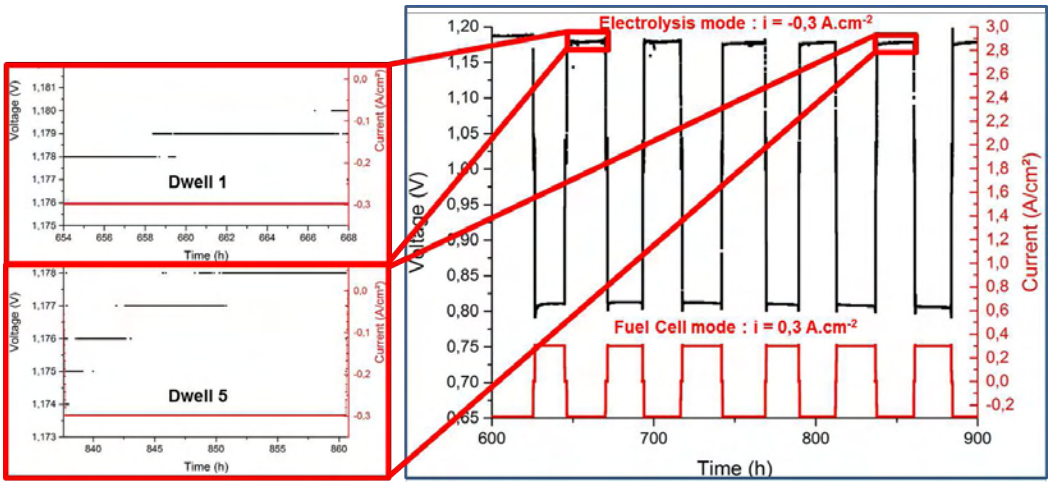

b.

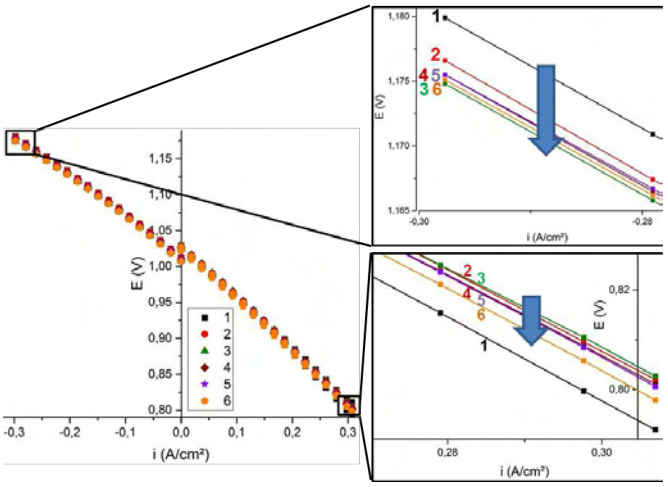

c.

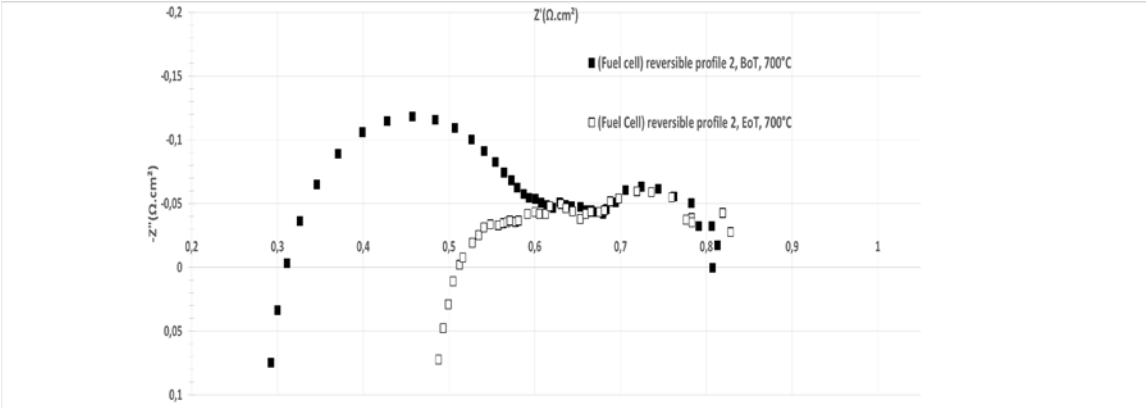

Figure 6. a) Polarization curve and b) Impedance spectra under polarization of a 16cm² sized NiO-BCZY81/BCZY81-ZnO/BSCF-BCZY81/BSCF cell during profile 2.

Profile 3 Electrochemical Characterizations

The BCZY81/BSCF-based cell is still running around 800 hours under static steam water electrolysis operation at -0.3 A/cm².

a.

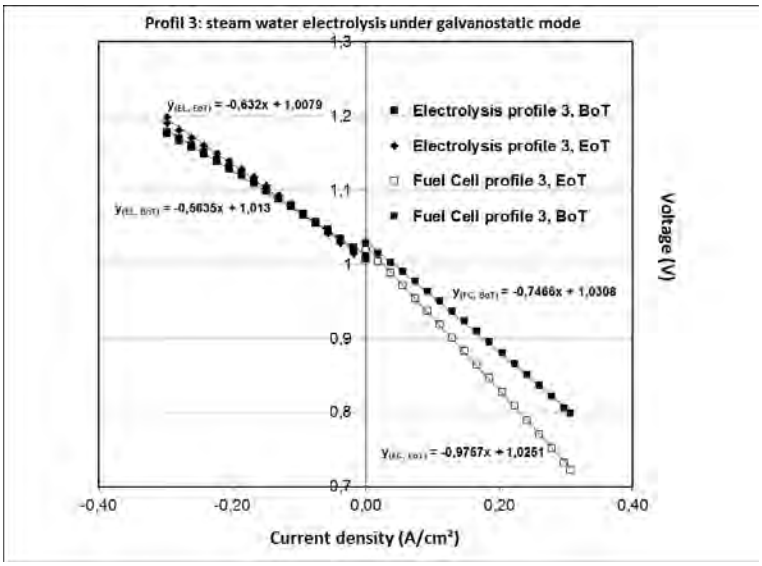

b.

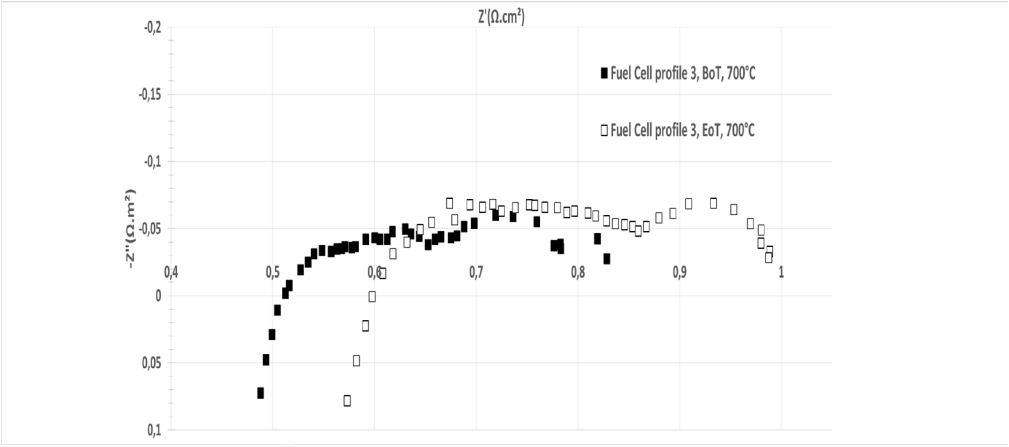

Figure 7. a) Polarization curve and b) Impedance spectra under polarization of a 16cm² sized NiO-BCZY81/BCZY81-ZnO/BSCF-BCZY81/BSCF cell during profile 3.

As observed for the profile 1 (for polarization resistance) and profile 2 (for ohmic resistance) tests, the analysis of impedance spectra before and after the test (figure 7b) reveals a slight increase of both ohmic and polarization resistances of the cell. That explains the relative decrease of cell performance measured with IV curves (figure 7a) and the electrical degradation of the cell voltage estimated to -6.2%/kh during such profile. Now, the electrical ageing of the cell would be mainly guided by the endurance time consumed (>1300h) and the exclusive negative impact of the high water partial pressure on the Ba-based material integrity.

Profile 4 Electrochemical Characterizations

The last operation test of the cell proposes to space out the reversible cycles steps and enlarge the galvanostatic fuel cell operation in order to deeper highlight the impact of the fuel cell mode on the electrical degradation of the cell with time. Nearly 2200h are realized during such profile.

a.

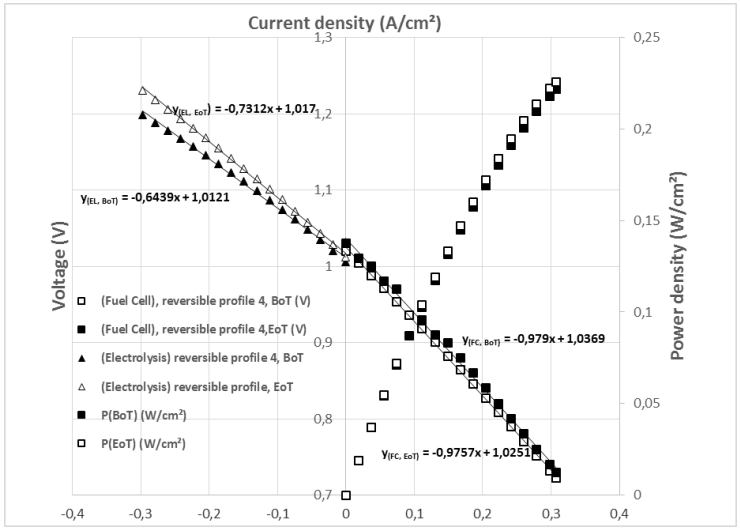

b.

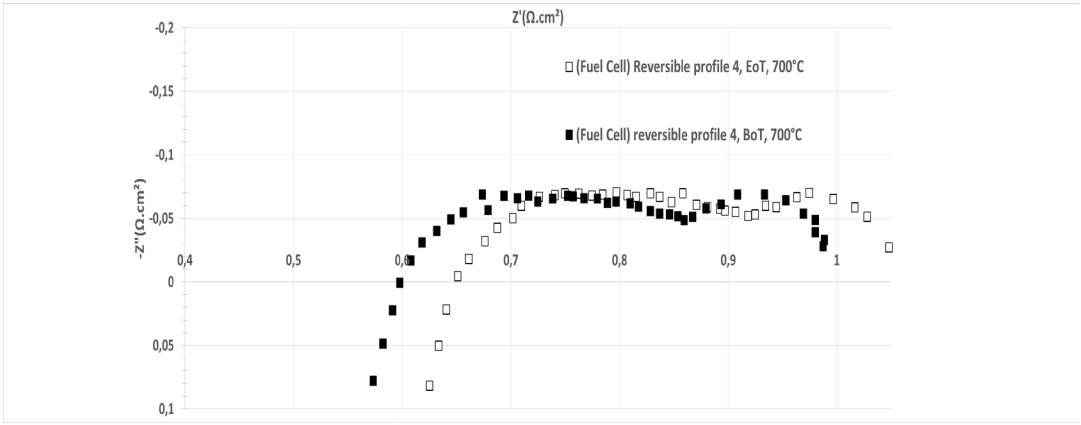

Figure 8. a) Polarization curve and b) Impedance spectra under polarization of a 16 cm² sized NiO-BCZY81/BCZY81-ZnO/BSCF-BCZY81/BSCF cell during profile 4.

The IV curves analysis of the figure 8 reveals no real electrical degradation under fuel cell mode and as confirmed by the relative stability of the total electrical resistance value of the cell within such profile. On the contrary, the electrolysis mode would induce a relative electrical degradation of cell performances. The cell would not suffer to the dynamic reversible cycle mode with an electrical degradation of cell voltage δV/V calculated to -0.5%/kh at 0.3 A/cm². Even more, the electrical aging of the cell voltage observed under the profile 3 (steam water electrolysis) seems to be reversible and could be linked to the choice of operation conditions (water steam pressure cycling, voltage cycling, inlet gases composition and temperature).

The Table II resumes the main value of OCV, ASR (ohmic, polarization) measured under different operation conditions of the endurance test:

TABLE II. OCV and ASRs 700°C vs. test operating conditions measured under current

Operation conditions	OCV (V)	IV-Curve	Electrochemical Impedance spectroscopy measurement @0.3 A/cm²			Pot. E @ -0.3A/cm² (V)
		ASR_{tot} ($\Omega.cm^2$)	ASR_{Ω} ($\Omega.cm^2$)	ASR_{pol} ($\Omega.cm^2$)	ASR_{tot} ($\Omega.cm^2$)	
Initial (Fuel cell)	1.03	0.79	0.63	0.41	1.04	0.81
Profile 1 (EoT) (Fuel Cell)	1.03	0.77	0.31	0.5	0.81	0.81
Profile 2 (EoT) (Fuel cell)	1.03	0.75	0.52	0.31	0.83	0.8
Profile 3 (EoT) Fuel cell	1.02	0.98	0.60	0.4	1.00	0.74
Profile 4 (EoT) Fuel cell	1.03	0.98	0.66	0.39	1.05	0.74

Finally, after 3500h of test under various operation conditions a very limited electrical degradation rate of -2%/1000h is measured with BCZY81/BSCF-based cell which confirms the relative good stability of such components under moderate water exposure, time consuming and polarization.

Post-tests Analysis

After the 3500 hours of test, SEM post-test observations are studied. As illustrated in the figure 9a, a good porosity and homogeneity of the hydrogen electrode is noticed. In addition, the BCZY81 electrolyte layer looks relatively thin (around 15 μm), dense (more than 95% determined by contrast image analysis) and is well adhered to both electrodes. A small degradation appears in the air electrode layers: bigger porosity can be seen near the interface with the electrolyte BCZY81 layer. The figure 9b illustrates the EDX analysis along the air electrode/electrolyte thickness. It can be also mentioned that no diffusion of elements between the three layers of the cell (composite interface/electrolyte/anode), in particular Ni element coming from cermet anode and Sr, Co, Fe coming from air electrode. Also, the presence of Ba element in the electrolyte confirms the excellent mechanical strength of BCZY81 material. The SEM/EDX observations are thus in accordance with the previous conclusions obtained from the analysis of impedance spectra and IV curves evolution of the cell, in particular concerning the increase of polarization resistance of the cell. However, deeper investigations with reproducible tests are needed to confirm the degradation mechanisms principles coming from electrodes.

a.

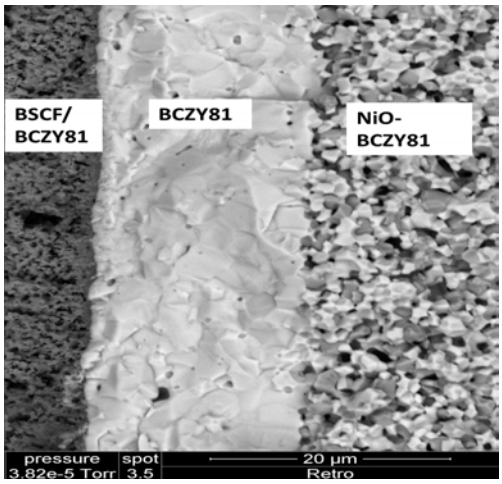

b.

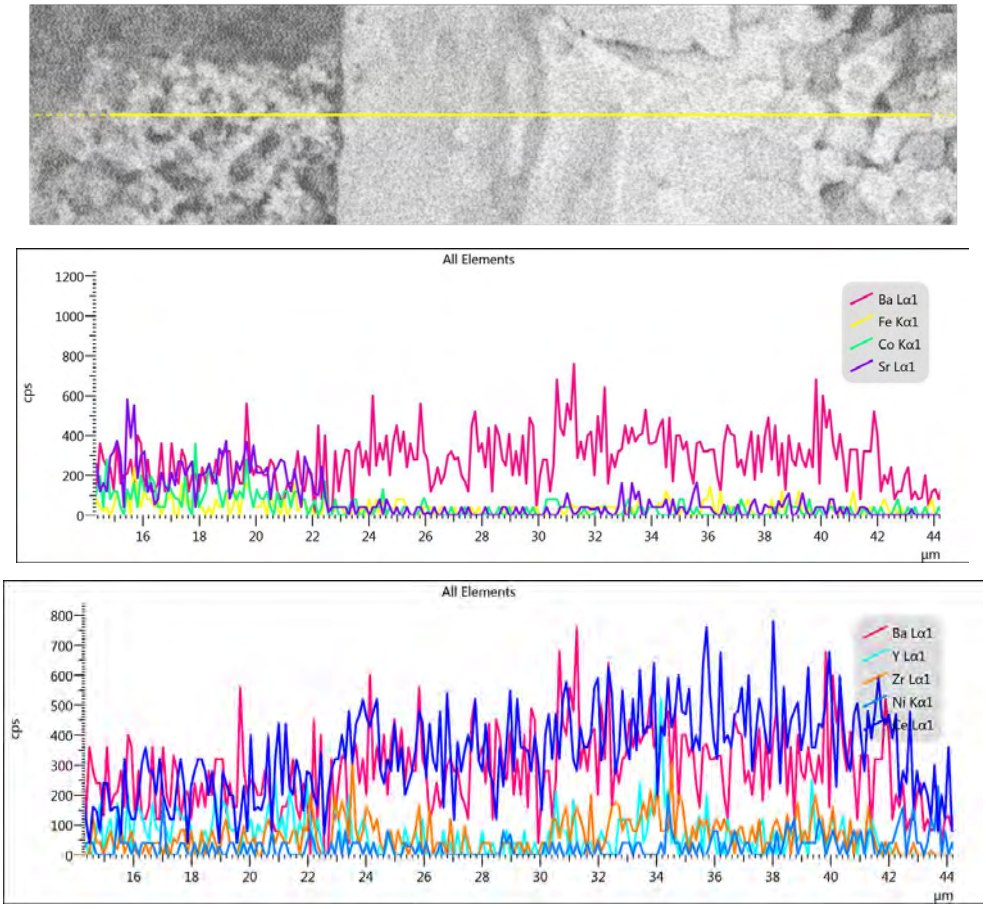

Figure 9. a) SEM images and b) EDX analysis of elements of the cell active layers.

Conclusion

All Ba-based PCC have been made using BCZY81 as electrolyte, NiO/BCZY81 as hydrogen electrode, BCZY81/BSCF as composite air electrode and BSCF as air current collector. Such 16 cm²-sized advanced PCC have been investigated under both

electrolysis and reversible fuel cell operation conditions. The influence of key parameters such as water feed content, fuel utilization and dynamic power demand profiles have been studied. Promising electrical cell performances under both fuel cell mode (>0.25 W/cm², 0.7V) and under steam water electrolysis mode (0.5A/cm², 1.3V) have been obtained during more than 3500h of duration test and a very limited electrical degradation rate of -2%/kh. In addition, the understanding of degradation mechanisms principles has been approached by using on-line impedance spectroscopy measurements and by post-test microscopy observations. Such study reveals that the initial total electrical resistances of cell layers are lower under electrolysis mode than under fuel cell mode, in particular the ohmic resistance. But in the same time, the polarization resistance of the cell is higher under electrolysis mode than under fuel cell mode. With time, the combination of high temperature and high water vapor pressure can induce conflict between an increase in proton conductivity of BCZY81 material used in the electrolyte and in the composite layers and the promotion of additive negative reaction with steam water able to accelerate the Ba-based materials aging. The post-test analysis confirms the excellent pioneer results of PCC in terms of mechanical strength and chemical stability of the system without any structural defects and chemical reactivity through PCC components layers. Thus, Ba-based perovskite materials can be considered as excellent candidates as protonic ceramic cell components to operate under both dynamic fuel cell and electrolysis cycling. Nevertheless, the choice of relevant operation conditions (inlet gases composition, steam water content, temperature and current) combined to well-tailored structures of PCC layers are fundamental to reach reliable and high performing cell operating under steam water electrolysis.

Acknowledgments

We would like to acknowledge Prof. G. Taillades and Dr. P. Pers of Charles Gerhardt Institute ICG-AIME Laboratory for their support to perform the SEM imaging and EDX analysis of the cell.

References

1. H. Iwahara, *Solid State Ionics*, **28-30**, 573 (1988).
2. W.G. Coors, *J. Power Sources,* **118**, 150 (2003).
3. G. Taillades, P. Pers, V. Mao, M. Taillades, *Int. J. Hydr. En.*, **41**, 12330 (2016).
4. G. Li, H. Jin, Y. Cui, L. Gui, B. He, L. Zhao, *J. Power Sources,* **341**, 192 (2017).
5. M. A. Azimova, S. McIntosh, *Solid State Ionics*, **203**, 57 (2011).
6. Y. Yoo and N. Lim, *Journal of Power Sources*, **229**, 48 (2013).
7. S. M. Babiniec, S. Ricote, N. P. Sullivan, *International Journal of Hydrogen Energy*, **40**, 9278 (2015).
8. S. Escolástico, J.M. Serra, *J. Membrane Science*, **489,** 112 (2015).
9. W. Deibert, F. Schulze-Küppers, E. Forster, M. E. Ivanova, M. Müller, W. A. Meulenberg, *J. European Ceramic Soc.,* **37**, 671 (2017).
10. Deibert, F. Schulze-Küppers, E. Forster, M. E. Ivanova, M. Müller, W. A. Meulenberg, *J. European Ceramic Soc.,* **37**, 671 (2017).

11. G. Taillades, J. Dailly, M. Taillades-Jacquin, F. Mauvy, A. Essouhmi, M. Marrony, C. Lalanne, S. Fourcade, D. J. Jones, J.-C. Grenier, J. Rozière, *Fuel Cells*, **10**, 166 (2010).
12. J. Dailly, M. Marrony, G. Taillades, M. Taillades-Jacquin, A. Grimaud, F. Mauvy, E. Louradour, J. Salmi, *Journal of Power Sources*, **255**, 302 (2014).
13. J. Dailly and M. Marrony, *Journal of Power Sources*, **240**, 323 (2013).
14. M. Marrony, M. Ancelin, G. Lefevre, J. Dailly, *Solid State Ionics*, **275,** 97 (2015).
15. J. Dailly, M. Marrony, *Solid State Ionics*, in press.
16. Y. Li, R. Guo, C. Wang, Y. Liu, Z. Shao, J. An, C. Liu, *Electrochim. Acta,* **95,** 95 (2013)
17. P. Colomban, O. Zaafrani, A. Slodczyk, *Membranes (Basel),* **2(3),** 493 (2012).
18. A. Slodczyk, O. Zaafrani, M.D. Sharp, J. A. Kilner, B. Dabrowski, O. Lacroix, P. Colomban, *Membranes (Basel),* **3(4),** 311 (2013).